Comparison of a new self developing photopolymer with AA/PVA based photopolymer utilizing the NPDD model

Michael R. Gleeson,[1,*] John T. Sheridan,[1] Friedrich-Karl Bruder,[2] Thomas Rölle,[2] Horst Berneth,[2] Marc-Stephan Weiser[2] and Thomas Fäcke[2]

[1]*UCD School of Electrical, Electronic and Mechanical Engineering, UCD Communications and Optoelectronic Research Centre, College of Engineering, Mathematical and Physical Sciences, University College Dublin, Belfield, Dublin 4, Ireland*

[2]*Bayer MaterialScience AG, IM – Functional Films – Competence Center Holographics / Optics&Surfaces, Leverkusen, Germany*

[*]*michael.gleeson@ucd.ie*

Abstract: The development of suitable recording media for applications such as holographic optical elements and holographic data storage are of significant research and commercial interest. In this paper, a photopolymer material developed by Bayer MaterialScience is examined using various optical techniques and then characterised using the Non-local Photo-polymerization Driven Diffusion model. This material demonstrates the capabilities of a new class of photopolymer offering high index modulation, full colour recording, high light sensitivity and environmental stability. One key result of this study is the material's high spatial frequency resolution, indicating a very low non-local effect, thus qualifying it as a very good storage medium.

OCIS codes: (050.1950) Diffraction gratings; (050.7330) Volume gratings; (090.2890) Holographic optical elements; (090.2900) Optical storage materials; (160.5335) Photosensitive materials; (160.5470) Polymers.

References and links

1. L. Dhar, A. Hale, H. E. Katz, M. L. Schilling, M. G. Schnoes, and F. C. Schilling, "Recording media that exhibit high dynamic range for digital holographic data storage," Opt. Lett. **24**(7), 487–489 (1999).
2. L. Dhar, A. Hale, K. Kurtis, M. Schnoes, M. Tackitt, W. Wilson, A. Hill, M. Schilling, H. Katz, and A. Olsen, "Photopolymer recording media for high density data storage," in Conference Digest, *Optical Data Storage, IEEE*, 158–160, (2000).
3. S. M. Schultz, E. N. Glytsis, and T. K. Gaylord, "Design, fabrication, and performance of preferential-order volume grating waveguide couplers," Appl. Opt. **39**(8), 1223–1232 (2000).
4. A. Sato, M. Scepanovic, and R. K. Kostuk, "Holographic edge-illuminated polymer Bragg gratings for dense wavelength division optical filters at 1550 nm," Appl. Opt. **42**(5), 778–784 (2003).
5. R. R. McLeod, A. J. Daiber, M. E. McDonald, T. L. Robertson, T. Slagle, S. L. Sochava, and L. Hesselink, "Microholographic multilayer optical disk data storage," Appl. Opt. **44**(16), 3197–3207 (2005).
6. T. D. Milster, "Horizons for optical storage," Optics and Photonics News **16**(3), 28–33 (2005).
7. J. T. Sheridan, J. V. Kelly, M. R. Gleeson, C. E. Close, and F. T. O'Neill, "Optimized holographic data storage: diffusion and randomization," J. Opt. A, Pure Appl. Opt. **8**(3), 236–243 (2006).
8. STX Aprilis Inc, *www.stxaprilis.com*, (2006 - 2008).
9. InPhase Technologies, www.inphase-technologies.com Tapestry Media, (2007).
10. M. Toishi, T. Tanaka, K. Watanabe, and K. Betsuyaku, "Analysis of photopolymer media of holographic data storage using non-local polymerization driven diffusion model," Jpn. J. Appl. Phys. Part 1-Regular Papers. Brief Communications. & Review. Papers. **46**(6A), 3438–3447 (2007).
11. Z. Nagy, P. Koppa, F. Ujhelyi, E. Dietz, S. Frohmann, and S. Orlic, "Modeling material saturation effects in microholographic recording," Opt. Express **15**(4), 1732–1737 (2007).
12. M. Toishi, T. Takeda, K. Tanaka, T. Tanaka, A. Fukumoto, and K. Watanabe, "Two-dimensional simulation of holographic data storage medium for multiplexed recording," Opt. Express **16**(4), 2829–2839 (2008).
13. S. Maruo, O. Nakamura, and S. Kawata, "Three-dimensional microfabrication with two-photon-absorbed photopolymerization," Opt. Lett. **22**(2), 132–134 (1997).

#151382 - $15.00 USD Received 26 Jul 2011; revised 5 Sep 2011; accepted 5 Sep 2011; published 9 Dec 2011

14. K. Saravanamuttu, C. F. Blanford, D. N. Sharp, E. R. Dedman, A. J. Turberfield, and R. G. Denning, "Sol-gel organic-inorganic composites for 3-D holographic lithography of photonic crystals with submicron periodicity," Chem. Mater. **15**(12), 2301–2304 (2003).
15. M. Straub, L. Nguyen, A. Fazlic, and M. Gu, "Complex-shaped three-dimensional microstructures and photonic crystals generated in a polysiloxane polymer by two-photon microstereolithography," Opt. Mater. **27**(3), 359–364 (2004).
16. A. C. Sullivan, M. W. Grabowski, and R. R. McLeod, "Three-dimensional direct-write lithography into photopolymer," Appl. Opt. **46**(3), 295–301 (2007).
17. G. Manivannan and R. A. Lessard, "Trends in holographic recording materials," Trends in Poly Sci. **2**, 282–290 (1994).
18. J. R. Lawrence, F. T. O'Neill, and J. T. Sheridan, "Photopolymer holographic recording material," Optik. Stuttgart. The. International. Journal. for. Light. And Electron. Optics. **112**(10), 449–463 (2001).
19. D. H. Close, A. D. Jacobson, R. C. Magerum, R. G. Brault, and F. J. McClung, "Hologram recording on photopolymer materials," Appl. Phys. Lett. **14**(5), 159–160 (1969).
20. Bayer MaterialScience AG, *www.bayermaterialscience.com*.
21. T. Rölle, F.-K. Bruder, T. Fäcke, M.-S. Weiser, D. Hönel and N. Stoeckel, "Photopolymerzusammensetzungen für optische Elemente und visuelle Darstellungen," EP2 172 505 A1, (2010).
22. H. Kogelnik, "Coupled wave theory for thick hologram gratings," Bell Syst. Tech. J. **48**(9), 2909–2945 (1969).
23. L. Solymar and D. J. Cooke, *Volume Holography and Volume Gratings*, Academic Press, London, (1981).
24. R. R. A. Syms, *Practical Volume Holography*, (Clarendon Press, Oxford, 1990).
25. G. H. Zhao and P. Mouroulis, "Diffusion-model of hologram formation in dry photopolymer materials," J. Mod. Opt. **41**(10), 1929–1939 (1994).
26. I. Aubrecht, M. Miler, and I. Koudela, "Recording of holographic diffraction gratings in photopolymers: Theoretical modelling and real-time monitoring of grating growth," J. Mod. Opt. **45**(7), 1465–1477 (1998).
27. C. R. Fernandez-Pousa, L. Carretero, and A. Fimia, "Dynamical behaviour of the optical properties of photopolymers and the Lorentz-Lorenz formula," J. Mod. Opt. **47**(8), 1419–1433 (2000).
28. M. R. Gleeson, S. Liu, S. O'Duill, and J. T. Sheridan, "Examination of the photoinitiation processes in photopolymer materials," J. Appl. Phys. **104**(6), 064917 (2008).
29. J. T. Sheridan and J. R. Lawrence, "Nonlocal-response diffusion model of holographic recording in photopolymer," J. Opt. Soc. Am. A **17**(6), 1108–1114 (2000).
30. M. R. Gleeson and J. T. Sheridan, "Non-local photo-polymerization kinetics including multiple termination mechanisms and dark reactions: Part I. Modelling," J. Opt. Soc. Am. B **26**(9), 1736–1745 (2009).
31. M. R. Gleeson, S. Liu, R. R. McLeod, and J. T. Sheridan, "Non-local photo-polymerization kinetics including multiple termination mechanisms and dark reactions: Part II. Experimental validation," J. Opt. Soc. Am. B **26**(9), 1746–1754 (2009).
32. M. R. Gleeson, S. Liu, J. Guo, and J. T. Sheridan, "Non-local photo-polymerization kinetics including multiple termination mechanisms and dark reactions: Part III. Primary radical generation and inhibition," J. Opt. Soc. Am. B **27**(9), 1804–1812 (2010).
33. M. R. Gleeson and J. T. Sheridan, "A review of the modelling of free-radical photopolymerisation in the formation of holographic gratings," J. Opt. A **10**, 024008 (2009).
34. G. Odian, *Principles of Polymerization*, Wiley, New York, (1991).
35. M. R. Gleeson, D. Sabol, S. Liu, C. E. Close, J. V. Kelly, and J. T. Sheridan, "Improvement of the spatial frequency response of photopolymer materials by modifying polymer chain length," J. Opt. Soc. Am. B **25**(3), 396–406 (2008).
36. F. T. O'Neill, A. J. Carr, S. M. Daniels, M. R. Gleeson, J. V. Kelly, J. R. Lawrence, and J. T. Sheridan, "Refractive elements produced in photopolymer layers," J. Mater. Sci. **40**(15), 4129–4132 (2005).
37. N. Suzuki, Y. Tomita, and T. Kojima, "Holographic recording in TiO_2 nanoparticle-dispersed methacrylate photopolymer films," Appl. Phys. Lett. **81**(22), 4121–4123 (2002).
38. J. V. Kelly, M. R. Gleeson, C. E. Close, F. T. O'Neill, J. T. Sheridan, S. Gallego, and C. Neipp, "Temporal analysis of grating formation in photopolymer using the nonlocal polymerization-driven diffusion model," Opt. Express **13**(18), 6990–7004 (2005).
39. C. E. Close, M. R. Gleeson, and J. T. Sheridan, "Monomer diffusion rates in photopolymer material. Part I. Low spatial frequency holographic gratings," J. Opt. Soc. Am. B **28**(4), 658–666 (2011).
40. C. E. Close, M. R. Gleeson, D. A. Mooney, and J. T. Sheridan, "Monomer diffusion rates in photopolymer material: part II: High frequency gratings and bulk diffusion," J. Opt. Soc. Am. B **28**(4), 842–850 (2011).
41. J. Guo, M. R. Gleeson, S. Liu, and J. Sheridan, "Non-local spatial frequency response of photopolymer materials containing chain transfer agents: I. Theoretical modelling," J. Opt. **13**(9), 095601 (2011).
42. J. Guo, M. R. Gleeson, S. Liu, and J. Sheridan, "Non-local spatial frequency response of photopolymer materials containing chain transfer agents: II. Experimental Results," J. Opt. **13**(9), 095602 (2011).
43. F. K. Bruder, F. Deuber, T. Fäcke, R. Hagen, D. Hönel, D. Jurbergs, T. Rölle, and M. S. Weiser, "Reaction diffusion model applied to high resolution Bayfol® HX photopolymer," Proc. SPIE **7619**, 76190I, 76190I-15 (2010).

#151382 - $15.00 USD Received 26 Jul 2011; revised 5 Sep 2011; accepted 5 Sep 2011; published 9 Dec 2011

1. Introduction

In recent decades, various media have been studied and developed for use in applications such as, holographic optical elements, holographic data storage [1–12], and hybrid photonic circuits [13–16]. Photopolymers are one of the most promising media of choice for such applications due to their versatility, ease of use, potential to be cast into thick layers having, environmental stability and self-processing ability. Such characteristics give them many advantages over more traditional materials examined in the literature, such as silver halide and di-chromated gelatine DCG [17,18]. In 1969 Close *et al*. [19] first introduced photopolymers as a potential holographic recording medium. Since then numerous systems have been examined and developed, but only a small number have become commercially available [8,9].

Recently, Bayer MaterialScience AG (BMS) [20], developed an acrylate based photopolymer material [21], suitable for many applications including the fabrication of optical lenses, mirrors, filters, waveguides, diffraction elements and other 3D image structures. Such acrylate photopolymer materials show great potential as holographic media owing to the high values of refractive index modulation and thus diffraction efficiency achievable. The BMS material that was investigated in this study represents one of many different photopolymer materials available for research and development purposes. Specifically this composition was designed to achieve high diffraction efficiency at ~50 μm film thickness for reflection recording geometries. This specific photopolymer film is of special interest in applications where a high spatial frequency and/or angle selectivity is required.

It is one of the aims of this paper to determine the suitability of this BMS photopolymer as a storage media. This is achieved by applying various optical and theoretical techniques, which have previously been presented in the literature [22–31]. The Non-local Photo-polymerisation Driven Diffusion (NPDD) model [29–32] is used in order to extract estimates of key material parameters from experimentally obtained data. These methods and results provide a quantitative basis to enable standardised comparisons to be made with existing and future recording media.

In order to place the performance of the BMS photopolymer in context, results for a well known acrylamide/polyvinylalcohol (AA/PVA) based photopolymer material [17, 28–33] are determined under equivalent conditions. In this way, the behaviour of key material parameters and characteristics can be highlighted.

The paper is structured as follows: In Section 2 the photochemical reactions, which occur during and post-exposure in photopolymers, are succinctly presented. Following this, the NPDD model used to evaluate the performance of the materials under examination is described based on these photochemical reactions. In Section 3 the composition, volume fractions and individual refractive indices of the main components of the BMS and AA/PVA photopolymers are presented. Section 4 describes the experimental procedures undertaken to quantify the relative performances of each of the materials being examined. From the various results obtained, values of the parameters which govern the behaviours of these materials are extracted using the NPDD model. The spatial frequency responses of both photopolymer materials are then examined and estimates of the non-local response length are provided based on fits to the experimental data. In Section 5 an overview of the results obtained and a brief conclusion are presented.

2. NPDD model

2.1 Photochemical Reactions

In 2009 a detailed review of the literature examining the modeling of the processes occurring during photo-polymerization was presented [33]. In this work, many of the assumptions made and limitation of models were discussed. In a series of papers [29–31], a number of these outstanding issues were dealt with through suitable extensions of the NPDD model. Crucially,

#151382 - $15.00 USD Received 26 Jul 2011; revised 5 Sep 2011; accepted 5 Sep 2011; published 9 Dec 2011

these developments yielded increased physicality, enabling a more accurate examination of a photopolymer material to be achieved. The availability of such a standardized method of quantitatively determining a given photopolymer's characteristics, allows more detailed direct comparison between different photopolymers, and provides a tool facilitating material optimization and improvement.

The photochemical reactions, which form the basis of the most recent NPDD model, are described in the flowchart presented in Fig. 1. These processes are separated into three main categories, *Initiation*, *Propagation* and *Termination* [34].

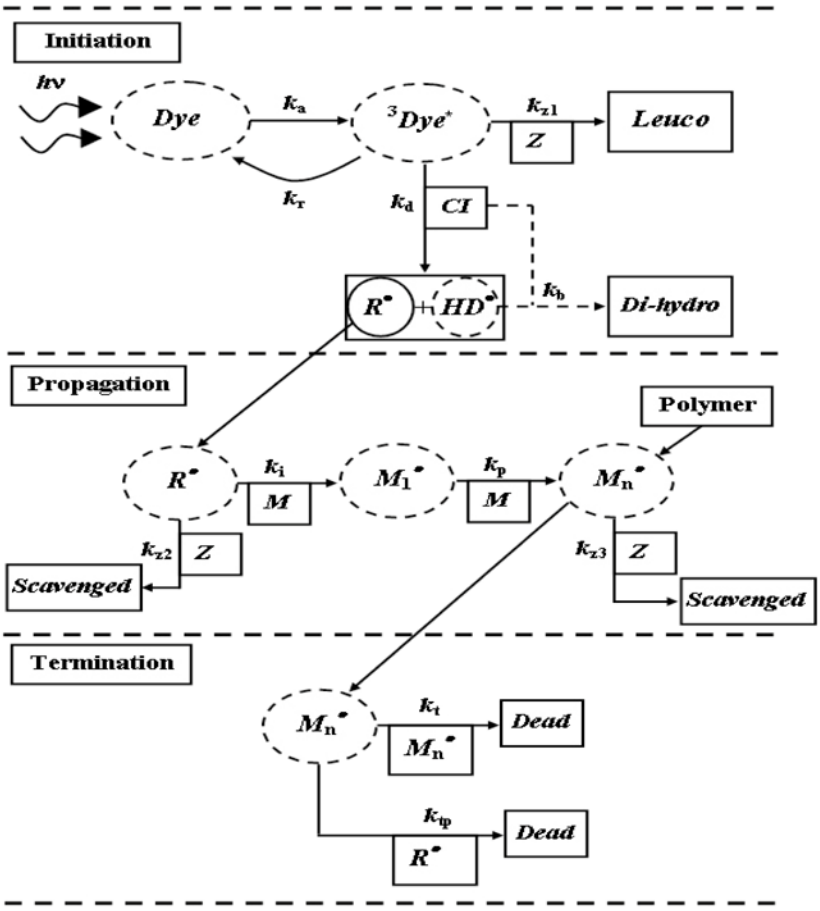

Fig. 1. Flowchart of the photochemical mechanisms, which take place during photopolymerisation.

In the flowchart, *hv* indicates the energy absorbed from a photon, *Dye* represents the ground state photosensitizer concentration, $^3Dye^*$ is the excited triplet state photosensitizer concentration, *CI* is the co-initiator concentration, $R^\bullet$ is the primary radical concentration, $HDye^\bullet$ represents a radicalized dye molecule, *M* is the monomer concentration, *Z* is the inhibitor concentration, $M_1^\bullet$ is a macroradical of length one, and $M_n^\bullet$ is a growing polymer chain with an active tip [34].

It is assumed that the term *Dead* signifies the cessation of the growth of a propagating macroradical [34], while the term *Scavenged* signifies the removal of a primary or macro-radical by an inhibitor, such as dissolved oxygen. k_a and k_r (s^{-1}) are the rates of excitation and recovery of the photosensitizer respectively and are assumed to contain all kinetic mechanisms involving the transferral of, *Dye*, to and from, $^3Dye^*$, such as intersystem crossing, fluorescence etc [28]. The rate constants associated with each of the chemical

#151382 - $15.00 USD Received 26 Jul 2011; revised 5 Sep 2011; accepted 5 Sep 2011; published 9 Dec 2011

reactions presented in the flowchart, k_i, k_p, k_t, k_{tp}, k_d, k_b, k_{z1}, k_{z2}, k_{z3} ($cm^3mol^{-1}s^{-1}$) are the rate constants of initiation, propagation, bimolecular termination, primary termination, dissociation, bleaching and inhibition respectively.

In order to use the proposed rate equations of the NPDD model, which are presented in Subsection 2.2, it is first necessary to convert the exposure intensity I_0 (mW/cm^2), for use in the model, to the appropriate units of Einsteins/cm^3s. This can be achieved as follows, $I_0' = \frac{T_{sf} B I_0}{d}\left(\frac{\lambda}{N_a hc}\right)$, where λ (nm) is the wavelength of incident light, N_a (mol^{-1}) is Avogadro's constant, c (m/s) is the speed of light, and h (Js) is Plank's constant. $B = 1 - e^{-\varepsilon A_0 d}$, is the absorptive fraction which determines a photopolymer material layer's initial absorptive capacity and is a function of the dye's initial concentration, A_0 (mol/cm^3), molar absorptivity, ε (cm^2/mol) and the material layer thickness, d (cm) [32]. T_{sf} is a fraction which represents the amount of light lost from scatter and Fresnel reflections.

The rate of production of the excited state photosensitizer, appearing in Fig. 1 can thus be represented by $k_a = \phi \varepsilon d I_0'$ (s^{-1}), where ϕ (mol/Einstein) is the quantum efficiency of the reaction [32]. Therefore, if the photosensitizer's initial concentration, molar absorptivity, quantum efficiency, and layer thickness are known, the rate of generation of excited state photosensitizer, $^3Dye^*$, can be determined for a given exposure intensity. The experimental methods used to obtain estimates of these parameters will be discussed later in Section 4 for both the BMS and the AA/PVA photopolymer materials examined here.

2.2 Coupled Differential Equations

During holographic illumination, there is a spatial distribution of irradiance, which in the case under examination in this paper is assumed to be typically co-sinusoidal. In this instance the incident intensity can be represented as $I(x,t) = I_0'\{1 + V\cos(Kx)\}$, where V is the fringe visibility and $K = 2\pi/\Lambda$, where Λ is the grating period. The mechanisms, which are presented in the flowchart in Fig. 1, can therefore be represented by a set of coupled differential equations, which contain both spatial and temporal variations of the concentrations of the components which makeup the materials.

The first order coupled differential equations representing the initiation processes presented in Fig. 1, are:

$$\frac{dDye(x,t)}{dt} = -k_a Dye(x,t) + k_r {}^3Dye^*(x,t), \tag{1}$$

$$\frac{d^3Dye^*(x,t)}{dt} = k_a Dye(x,t) - k_r {}^3Dye^*(x,t) - k_d {}^3Dye^*(x,t) CI(x,t) - k_{z1} {}^3Dye^*(x,t) Z(x,t), \tag{2}$$

$$\frac{dCI(x,t)}{dt} = -k_d {}^3Dye^*(x,t) CI(x,t) - k_b HDye^\bullet(x,t) CI(x,t), \tag{3}$$

$$\frac{dHDye^\bullet(x,t)}{dt} = k_d {}^3Dye^*(x,t) CI(x,t) - k_b HDye^\bullet(x,t) CI(x,t), \tag{4}$$

As in the previous analyses [30–32], it is assumed that the effect of inhibition during exposure is due solely to dissolved oxygen which is initially present within the photopolymer layer and oxygen which may diffuse in from the surrounding environment. In reality the chemicals, which constitute the photopolymer material may contain various additives, which

#151382 - $15.00 USD Received 26 Jul 2011; revised 5 Sep 2011; accepted 5 Sep 2011; published 9 Dec 2011

are added to increase shelf life. These stabilising components also have inhibiting properties however these are neglected in this analysis.

The non-uniform recording irradiance, i.e., the co-sinusoidal exposing intensity distribution produces photochemical reactions which cause concentration gradients resulting in the diffusion of inhibiting oxygen from the dark non-illuminated regions to the bright illuminated regions. As oxygen molecules are small compared to the surrounding material, it can be assumed that the oxygen is relatively free to diffuse rapidly, resulting in a one-dimensional standard diffusion equation governing the inhibitor concentration,

$$\frac{dZ(x,t)}{dt} = \frac{d}{dx}\left[D_z \frac{dZ(x,t)}{dx} \right] - k_{z1}{}^3 Dye^*(x,t) Z(x,t) - k_{z2} Z(x,t) R^\bullet(x,t) - k_{z3} Z(x,t) M^\bullet(x,t) + \tau_z \left[Z_0 - Z(x,t) \right], \tag{5}$$

where Z is the instantaneous inhibiting oxygen concentration and D_z is the diffusion coefficient of oxygen in the material layer, which will be assumed to be time and space independent. τ_z represents the rate of replenishing of oxygen from outside the material layer. We note that it is assumed that the oxygen concentration in the layer can never be larger than the original dissolved oxygen concentration, Z_0 (mol/cm^3) and that this additive term is assumed to be independent of position [32].

As in the previous analyses in the literature it is assumed for simplicity that, $k_{z2} = k_{z3} = k_z$ [30–32], although in general it would be expected that the inhibition rate constants would have different values (of reactivity) due to the differences in the relative molecular size [34]. Furthermore it is expected that the reactivity of oxygen with the excited triplet state form of the photosensitiser will be much lower, i.e., $k_{z1} << k_z$, and therefore we assume it is negligible in this analysis, i.e., $k_{z1} = 0$. As was previously assumed the inhibition rate constant can be expressed as [30–32],

$$k_z = k_{z,0} \exp\left(-E_z / RT\right), \tag{6}$$

where in this equation $k_{z,0}$ (cm^{3}mol^{-1}s^{-1}) is the Arrhenius pre-exponential factor, E_z = 18.23×10^3 (Jmol^{-1}) is the activation energy of oxygen, R = 8.31 (JK^{-1}mol^{-1}) is the universal gas constant, and T (K) is the ambient temperature.

The equation governing the concentration of primary radicals, including the newly added term for primary radical generation [32], is given by

$$\frac{dR^\bullet(x,t)}{dt} = k_a{}^3 Dye^*(x,t) CI(x,t) - k_i R^\bullet(x,t) u(x,t) - k_{tp} R^\bullet(x,t) M^\bullet(x,t) - k_z R^\bullet(x,t) Z(x,t), \tag{7}$$

where $u(x, t)$ is the free-monomer concentration, (denoted earlier in the flowchart by M). This equation states that the rate of change of primary radical concentration is equal to the concentration of primary radicals generated by photon absorption, less the amounts removed by the initiation of macroradicals, primary termination with growing polymer chains, and inhibition by dissolved oxygen.

Incorporating both types of termination mechanism presented in Fig. 1, i.e., primary and bimolecular termination, the equation governing the temporal and spatial macroradical concentration is then given as,

$$\frac{dM^\bullet(x,t)}{dt} = k_i R^\bullet(x,t) u(x,t) - k_t \left[M^\bullet(x,t) \right]^2 - k_{tp} R^\bullet(x,t) M^\bullet(x,t) - k_z Z(x,t) M^\bullet(x,t), \tag{8}$$

#151382 - $15.00 USD Received 26 Jul 2011; revised 5 Sep 2011; accepted 5 Sep 2011; published 9 Dec 2011

where the squared term represents the effects of bimolecular termination. The generation term in this equation previously appears as the removal term due to macroradical initiation in Eq. (7).

In the same manner as discussed above in relation to the inhibitor, the non-uniform irradiance distribution creates monomer concentration gradients, and as a result monomer diffuses from the dark regions to the monomer depleted exposed regions. This results in a periodic polymer concentration distribution, and a modulation of refractive index in the material, i.e., the holographic grating. We represent the monomer concentration using the following 1-D diffusion equation,

$$\frac{du(x,t)}{dt} = \frac{d}{dx}\left[D_m(x,t)\frac{du(x,t)}{dx} \right] - k_i R^{\bullet}(x,t)u(x,t) - \int_{-\infty}^{\infty} k_p M^{\bullet}(x',t)u(x',t)G(x,x')dx', \tag{9}$$

where $D_m(x, t)$ represents the monomer diffusion. $G(x,x')$ is the non-local material spatial response function given by:

$$G(x,x') = \frac{1}{\sqrt{2\pi\sigma}}\exp\left[\frac{-(x-x')^2}{2\sigma} \right], \tag{10}$$

where σ is the constant non-local response parameter normalized with respect to the grating period, Λ [29]. This non-local spatial response function represents the effect of a chain initiation at location x' on the amount of monomer polymerized at location x [29–32]. This is an important parameter when considering the data storage capacity or recording resolution of a photopolymer. These materials high spatial frequency responses will be addressed later in the paper.

One point to note is that the non-local response of a given photopolymer is produced by a combination of several physical effects, which result in the smearing of the grating being recorded in the photopolymer. One such smearing effect is the growth of polymer chains away from the point of their initiation, into the dark less exposed regions of the material layer. This propagation out of the bright regions causes an increase in the average refractive index of the dark region and as a result, reduces the overall refractive index modulation achievable. This has been illustrated in discussed in detail in previous publications [30–32,35], and is more significant when recording high spatial frequency.

The equation governing the polymer concentration is given by,

$$\frac{dN(x,t)}{dt} = \int_{-\infty}^{\infty} k_p M^{\bullet}(x',t)u(x',t)G(x,x')dx' - \frac{d}{dx}\left[D_N(x,t)\frac{dN(x,t)}{dx} \right], \tag{11}$$

where $D_N(x, t)$ represents the polymer diffusion. As with the monomer, Eq. (9), the non-uniform irradiance creates a polymer concentration distribution. If the polymer chains are not cross-linked sufficiently, they will tend to diffuse out of the exposed regions in order to reduce the polymer concentration gradient. If this takes place the grating strength will decay with time. However in this study, as is evident from the experimental results presented later, we assume there is sufficient cross-linking so that $D_N(x,t) = 0$, i.e., the gratings recorded are stable.

We note at this point that it is assumed that both the primary and macro-radicals generated during exposure are consumed so rapidly that there is insufficient time for them to diffuse away from their point of initiation. It is for this reason that we have not added diffusion terms in Eqs. (7) and (8).

#151382 - $15.00 USD Received 26 Jul 2011; revised 5 Sep 2011; accepted 5 Sep 2011; published 9 Dec 2011

Since all the above equations presented, i.e., Eqs. (1-5), (7-9) and (11) are derived assuming a cosinusoidal spatial distribution of the exposing intensity, they will all be periodic even functions of x and can be written as Fourier series, i.e., $X(x,t) = \sum_{j=0}^{\infty} X_j(t)\cos(jKx)$, where X represents the species concentrations, Dye, $^3Dye^*$, CI, $HDye^\bullet$, $R^\bullet$, $M^\bullet$, u, N and Z.

A set of first-order coupled differential equations can then be obtained by gathering the coefficients of the various co-sinusoidal spatial frequencies and writing the equations in terms of these time varying spatial harmonic amplitudes [30–32]. These coupled equations are then solved assuming the following initial conditions:

$$\begin{aligned} &Z_0(t=0) = Z_0,\ Dye_0(t=0) = Dye_0,\ CI_0(t=0) = CI_0,\ u_0(t=0) = U_0, \\ &Dye_{n>0}(t=0) = {}^3Dye^*_{n\geq 0}(t=0) = HDye^\bullet_{n\geq 0}(t=0) = CI_{n>0}(t=0) = 0, \text{ and} \\ &Z_{n>0}(t=0) = R^\bullet_{n\geq 0}(t=0) = M^\bullet_{n\geq 0}(t=0) = N_{n\geq 0}(t=0) = 0. \end{aligned} \quad (12)$$

As in previous papers [29–32, 35], the equations governing the monomer and polymer harmonics include the effects of the non-local response parameter $G(x,x')$, represented in the coupled differential equations by $S_i = \exp\left(-i^2K^2\sigma/2\right)$.

3. Photopolymer materials

In this section the volume fractions and associated refractive indices of the main components of the BMS and AA/PVA photopolymer materials are presented. It is necessary to obtain these values so that the temporal evolution of the refractive index modulation can be predicted using the Lorentz-Lorenz relation [26, 27, 30–32, 35], which is discussed later in the results section. Full details of the preparation and fabrication procedures of the BMS and AA/PVA photopolymers are provided in [21] and [28] respectively and will not be repeated here.

3.1 Volume fraction analysis

As described in [26, 27, 30–32, 35], the Lorentz-Lorenz relation can be used to determine the variation of the refractive index of the photopolymer. In order to do so, the volume fractions and refractive indices of the individual components of the photopolymer must be known. By making the assumption that the overall volume of the material is conserved, (in itself a topic of debate in the literature [33]), the volume fraction of each component can be expressed as $\phi_i = x_i v_i / \sum_i x_i v_i$, where x_i is the mole fraction and v_i is the molar volume of the i^{th} component. In this case,

$$\phi^{(m)}(t) + \phi^{(p)}(t) + \phi^{(b)}(t) = 1, \quad (13)$$

where $\phi^{(m)}$, $\phi^{(p)}$ and $\phi^{(b)}$ are the respective volume fractions of the monomer, polymer and background material. For both of the photopolymers analyzed, it is assumed that the background material consists of the respective matrix binder, co-initiator and photosensitiser. The volume fractions and concentrations (mol/cm^3) of each of the components which constitute the BMS photopolymer are presented in Table 1.

Table 1. Volume fractions and concentrations of the main components of the BMS acrylate photopolymer material. Concentration of matrix unavailable.

Component	Volume Fraction	Concentration (mol/cm^3)
Monomer	0.2500	3.08×10^{-4}
Matrix	0.7467	-
Dye	0.0003	8.55×10^{-7}
Co-initiator	0.0030	4.20×10^{-6}

#151382 - $15.00 USD Received 26 Jul 2011; revised 5 Sep 2011; accepted 5 Sep 2011; published 9 Dec 2011

The corresponding values for the AA/PVA photopolymer are presented in Table 2.

Table 2. Volume fractions and concentrations of the main components of the acrylamide/polyvinylalcohol photopolymer material. Concentration of matrix unavailable.

Component	Volume Fraction	Concentration (mol/cm^3)
Monomer	0.1720	2.83×10^{-3}
Matrix	0.3326	-
Dye	0.0011	1.22×10^{-6}
Co-initiator	0.4942	3.28×10^{-3}

One of the key differences between the two materials being examined is the matrix. In the BMS system, a two-step polymerization process is used. The first polymerization process involves thermally curing the binder (matrix), which then hosts the other components of the material, in a stable network (rigid layer). This network yields a number of advantages such as: (i) Minimizing volume fluctuations, i.e., < 1.1% shrinkage, (ii) Increasing the validity of the assumption made in Eq. (13), that volume is conserved during and post photo-polymerisation; and (iii) Reducing detrimental environmental effects such as humidity and inhibition as the layers can be sealed. The second polymerization process in the acrylate system is photo-polymerization which enables the holographic recording.

In the AA/PVA material, the matrix is more gel like and consequently not as rigid as the BMS system. This matrix therefore offers significantly reduced stability and suffers from large material shrinkage as a result of polymerization and mass transport effects [36]. This network is also susceptible to environmental effects and so procedures such as cover-plating (sealing the material with a cover layer) are crucial [33].

As mentioned earlier, much work has been presented in the literature with the aim of: (i) reducing the effects of material shrinkage [37], and (ii) developing a model which accurately predicts the changes associated with these shrinkage effects [38]. However, in the analysis presented in this paper, involving the recording of unslanted transmission type gratings for which volume variations will have a minimal effect, we neglect thickness changes and assume that volume is conserved.

3.2 Indices of refraction

In order to obtain accurate values for the refractive indices of the components of both materials under examination we utilised a number of methods. In order to determine the refractive index of the BMS photopolymer before and after thermal curing, 100 - 300 nm thick samples were made by spin coating the material on quartz glass substrates from dilute solution in Butyl Acetate. The transmission and reflection spectrum of each layer was measured using a spectrometer, and the layer thickness and the spectral curve of refractive index were then estimated from the measured transmission and reflection spectra. This automatic processing of the measured data required that the refractive index of the quartz glass substrate be known and this was determined separately by performing a blank measurement. The resulting value for the material's refractive index before flood curing, n_s^{bfc} is presented in Table 3.

Table 3. Refractive indices of the main components of the BMS acrylate photopolymer material.

Component	Refractive Index
n_m	1.575
$n_{b@589nm}$	1.482
n_s^{bfc}	1.498
n_s^{afc} (n_{dark})	1.503
$n_{p@UV}$	1.590

#151382 - $15.00 USD Received 26 Jul 2011; revised 5 Sep 2011; accepted 5 Sep 2011; published 9 Dec 2011

The same procedure was carried out in order to obtain the refractive index of the material after thermal flood curing, n_s^{afc}, which is also referred to as, n_{dark}, see Table 3. n_{dark} represents the refractive index of the acrylate photopolymer material before exposure.

As stated earlier, the acrylate photopolymer material consists of *four* main components, a photosensitiser, a co-initiator, a monomer and a binder, see Table 1. Since the volume fractions of the co-initiator and photosensitiser are small in comparison to that of the monomer and the matrix binder, their contribution is treated as being part of the background material. Therefore, only the refractive indices of the monomer, background and polymer, (which were measured using a refractometer), are presented. These values are listed in Table 3, where n_m is the refractive index of the monomer, n_b is the refractive index of the background (matrix with residual components), and n_p is the refractive index of the polymerised monomer.

Using the method described in [30, 35], the refractive indices of the main components of the AA/PVA photopolymer were measured and are listed in Table 4. All measurements were carried out at $\lambda = 633$ nm which is the replay probe beam wavelength used to monitor grating growth in Section 5.

Table 4. Refractive indices of the main components of the AA/PVA photopolymer material.

Component	Refractive Index
n_m	1.472
$n_{b@633nm}$	1.496
n_{dark}	1.498
$n_{p@633nm}$	1.520

Having obtained the volume fractions and refractive indices of the various components which constitute each of the materials under examination, it becomes possible to determine the temporal evolution of the refractive index modulation of the gratings recorded. However, in order to accurately predict the response of each material to a given holographic exposure, it is necessary to first examine each material's absorptive behaviour.

4. Experimental and theoretical analysis

In this section we present the various experimental and theoretical procedures taken, in order to make meaningful comparisons between the two photopolymer materials under examination. Although the photo-kinetic processes which take place during holographic exposure occur simultaneously, we begin by separately measuring each physical process using different optical techniques and then analyse them independently. In this way, we can quantify the behaviours of the different processes in the materials and isolate their individual contribution to the formation of the holographic grating. Understanding the combined results of these effects enables each material to be fully characterised. In this way, meaningful quantitative comparisons can then be made between the photopolymer materials under examination.

4.1 Experimental setup

4.1.1 Refractive index modulation

Figure 2 shows a schematic diagram of the experimental setup used to record and monitor the temporal evolution of the refractive index modulation of the gratings being formed. As both photopolymers under examination are self-processing (i.e., are non-latent), the diffraction efficiency of the gratings can be measured during recording. Thus the formation of the grating can be monitored using the intensity values from detectors D_1 and D_2 (in Fig. 2), by replaying the grating as it is being recorded using weak probe laser beams of wavelength 633 nm (HeNe), which lies outside the absorption spectrum of the photosensitizers used.

#151382 - $15.00 USD Received 26 Jul 2011; revised 5 Sep 2011; accepted 5 Sep 2011; published 9 Dec 2011

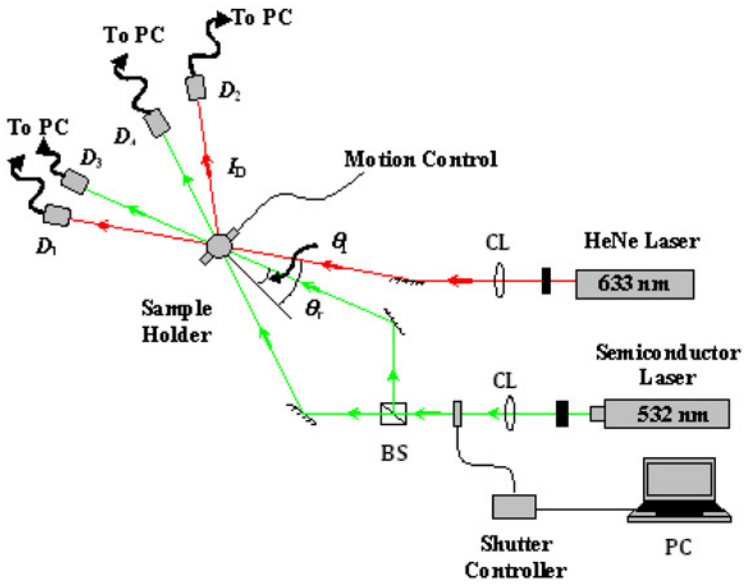

Fig. 2. Typical experimental set-up used to record unlsanted volume transmission holographic gratings with a recording wavelength of λ = 532 nm.

Then, using Kogelnik's two-wave coupled wave theory [22], the ratio of the incident and diffracted probe beam intensities, i.e., the diffraction efficiency, η, describes the strength of the grating modulation as its is being formed. For a lossless, unslanted transmission geometry grating, replayed on-Bragg with TE polarized probe light, $\eta(t)$ is described by the following equation:

$$\eta(t) = \frac{I_D(t)}{I_{in}} = \sin^2\left[\frac{\pi n_1(t) d}{\lambda \cos\theta}\right], \tag{14}$$

where I_{in} and $I_D(t)$ are the incident and diffracted probe beam intensities respectively, d represents grating thickness, θ and λ are the Bragg angle and wavelength of incident probe beam inside the grating, and $n_1(t)$ is the refractive index modulation (first spatial harmonic amplitude). In deriving Eq. (14) all boundary reflections have been neglected.

Rearranging Eq. (14) enables an expression for the temporally varying refractive index modulation, $n_1(t)$, obtained from $\eta(t)$,

$$n_1(t) = \frac{\lambda \cos\theta}{\pi d} \sin^{-1}\left[\sqrt{\eta(t)}\right]. \tag{15}$$

In order to accurately apply the NPDD model described in Section 2 we apply the Lorentz-Lorenz relation using the volume fractions and refractive indices of each of the material components presented in Tables 1 - 4. The temporal evolution of the refractive index modulation can then be described by,

$$n_1(t) = \frac{\left(n_{dark}^2 + 2\right)^2}{6 n_{dark}} \left[\phi_1^{(m)}(t)\left(\frac{n_m^2 - 1}{n_m^2 + 2} - \frac{n_b^2 - 1}{n_b^2 + 2}\right) + \phi_1^{(p)}(t)\left(\frac{n_p^2 - 1}{n_p^2 + 2} - \frac{n_b^2 - 1}{n_b^2 + 2}\right)\right], \tag{16}$$

where $\phi_1^{(m)}(t)$ and $\phi_1^{(p)}(t)$ are the time varying first harmonic volume fraction components of monomer and polymer respectively. Our process to characterise the materials and estimate parameter values involves generating these volume fraction components directly using the NPDD model. Applying a least squares fitting algorithm, the difference between the

#151382 - $15.00 USD Received 26 Jul 2011; revised 5 Sep 2011; accepted 5 Sep 2011; published 9 Dec 2011

experimentally obtained growth curve data and the predictions of the NPDD model are iteratively minimized by allowing the 'unknown' parameter values to vary over physically reasonable search ranges. From the resulting best fit, estimates are obtained for the various kinetic rates which quantitatively describe the material's performance.

In addition, by placing the photosensitive sample on a rotation stage (see Fig. 2), the angular response of the grating, once it has been formed can be examined. From such measurements the grating strength and the material thickness can be confirmed and the grating uniformity discussed.

4.1.2 Absorption

All the results reported in this paper are for unslanted volume transmission type gratings. During grating fabrication the temporal variation of the transmitted recording beams are monitored using photo-detectors D_3 and D_4, as shown in Fig. 2. As discussed in Section 2.1 the absorption of the exposing light by the photosensitiser, and the subsequent production of primary radicals, drives the photo-polymerisation process. In order to determine the quantity of photons which are absorbed during recording we simply relate the fraction of the recording beams transmitted to the total amount which is incident (corrected for Fresnel losses) [32]. Then by fitting the resulting normalised transmission curves using the model presented in Section 2, estimates for the values of, ϕ, ε and d can be made. Using these, the rate of production of the excited state photosensitiser, k_a (s^{-1}), can then be determined.

4.2 Experimental results

A combination of the above experimental techniques was carried out to examine both the AA/PVA and BMS photopolymer materials, for a range of exposure intensities and spatial frequencies. In all cases a solid state crystal laser, $\lambda = 532$ nm, and HeNe probe laser, $\lambda = 633$ nm, were used, and the fringe visibility of the recording interference pattern was $V = 1$. The growth curve data was then processed using Eq. (15) and the NPDD model was applied to estimate various material parameter values. We now present the results for the two photopolymers.

4.2.1 AA/PVA photopolymer

Growth curves of refractive index modulation were recorded in AA/PVA photopolymer for a range of exposure intensities; $I_{01} = 1$ mW/cm^2, $I_{02} = 4$ mW/cm^2 and $I_{03} = 8$ mW/cm^2. During each holographic exposure, the time evolution of: (i) the transmitted recording beams, and (ii) the transmitted and diffracted probe beams, were monitored. In order to ensure experimental reproducibility each recording was repeated several times. After each recording, the material was allowed to rest in the dark for several minutes allowing post-exposure effects to take place, (dark reactions: continued chain growth, diffusion etc.). The angular response of each recording was then captured by rotating the material relative to the incident probe beam. This process was then repeated for a range of spatial frequencies from, $500 \le SF = 1/\Lambda \le 3000$ lines/mm.

The NPDD model, presented in Section 2, was then applied to fit the experimental data. Table 5 shows the various dye absorption parameters extracted from fits to the normalised transmission curve data recorded for the exposure of intensity $I_{03} = 8$ mW/cm^2, for the spatial frequencies examined. As can be seen from the table, there is good general agreement between the values obtained for the absorption parameters at the various spatial frequencies. These values are also consistent with those previously reported in the literature [28, 30–32, 35]. From the estimates obtained for the quantum efficiency and molar absorptivity, values for the rate of production of the excited state photosensitiser, k_a (s^{-1}), were then obtained and are also provided in Table 5. As k_a is proportional to the exposure intensity used, its value decreases for each of the lower exposure intensities used, i.e., $I_0 = 1$ and 4 mW/cm^2.

#151382 - $15.00 USD Received 26 Jul 2011; revised 5 Sep 2011; accepted 5 Sep 2011; published 9 Dec 2011

Table 5. Parameters extracted from normalised transmission curves over a range of spatial frequencies in the AA/PVA photopolymer material. I_0 = 8 mW/cm^2.

Spatial Frequency (lines/mm)	T_0	T_{sf}	ε ($\times 10^8$) (cm^2/mol)	ϕ (mol/Einstein)	k_a (cm^3/mol s)
500	0.15	0.85	1.421	0.035	0.1242
1000	0.16	0.84	1.430	0.035	0.1214
1428	0.16	0.84	1.359	0.035	0.1153
2000	0.18	0.85	1.413	0.035	0.1182
2500	0.18	0.84	1.402	0.035	0.1155
3000	0.15	0.84	1.344	0.035	0.1158
Mean	**0.16±0.02**	**0.84±0.01**	**1.394±0.05**	**0.035**	**0.1184±0.0058**

The thickness of the material layers, d (μm), was extracted from fits to the recorded angular scan data using Kogelnik's expression for Off-Bragg replay [22]. These thickness values (d = 97 ± 8 μm) were then used to extract the refractive index modulation from the diffraction efficiency using Eq. (15). The growth curves are fit then using the NPDD model. Note that the change in the optical path length that the recording beams 'see' as a result of the change in the incident angle, which occurs when the spatial frequency is increased, is fully accounted for in the model.

Table 6 lists the extracted parameter values obtained for the AA/PVA material when the growth curves were fit using the NPDD model for each of the spatial frequencies examined. The spatial frequency values used are given in the first column along with the saturation values of refractive index modulation achieved which are presented in square brackets. The estimated parameters obtained from the fits are, the rate of dissociation of the initiator, k_d, the propagation rate, k_p, the bimolecular termination rate, k_t, the monomer diffusion rate, D_{m0} and the nonlocal response length, $\sqrt{\sigma}$ (nm). In all cases, it was assumed that the initiation and propagation rates are equal, i.e., $k_i = k_p$. In essence this means that it is being assumed that the rate at which a primary radical reacts with a monomer is the same as the rate a macro-radical reacts with a monomer. This is not an unlikely scenario even when the relative sizes of the molecules are considered [34]. We also make the assumption that the primary termination rate $k_{tp} = 10 \times k_t$. This relationship is assumed based on the results of previous best fits and lies within the reasonable range of values indicated in the literature [34].

Examining the values presented in Table 6, it can be seen that there is no significant change in the values obtained for the different spatial frequencies. It is important to note the relative consistency of the values obtained for the monomer diffusion constant and the nonlocal response parameter. In the case of monomer diffusion, the values extracted are very much in agreement with the majority of estimates and measurements appearing in the literature [30–32, 39, 40]. As has been observed this AA/PVA material, suffers significantly from nonlocal effects. The mean value presented in Table 6 for the nonlocal response parameter $\sqrt{\sigma}$ ≈61.3 nm, which is consistent with values previously presented [35]. In order to indicate the quality of the fits achieved using these parameter estimates, Mean Squared Error (MSE) values are provided in the right hand most column.

#151382 - $15.00 USD Received 26 Jul 2011; revised 5 Sep 2011; accepted 5 Sep 2011; published 9 Dec 2011

Table 6. Parameters extracted from growth curves of refractive index modulation over a range of spatial frequencies in the AA/PVA photopolymer material.

SF (lines/mm) [$n_1^{sat}\times10^{-3}$]	k_d $cm^3/mols$ ($\times10^3$)	k_p $cm^3/mols$ ($\times10^7$)	k_t $cm^3/mols$ ($\times10^8$)	D_{m0} cm^2/s ($\times10^{-11}$)	$\sqrt{\sigma}$ nm	MSE ($\times10^{-10}$)
500 [2.07]	1.60	2.7	3.0	3.0	60	1.96
1000 [2.20]	1.61	2.3	3.6	1.0	68	1.64
1428 [2.36]	1.53	2.8	3.0	3.0	55	0.89
2000 [1.97]	1.60	2.2	3.8	2.0	60	1.09
2500 [1.56]	1.55	2.7	3.1	3.0	65	1.21
3000 [1.38]	1.58	2.6	3.2	3.0	60	2.72
Mean	**1.58±0.05**	**2.6±0.4**	**3.3±0.5**	**2.5±1.5**	**61±6.7**	**1.59±1.13**

Figure 3 demonstrates the consistent quality of the fits obtained. Three growth curves for exposure intensities are, I_{01} = 1 mW/cm^2 (red triangles), I_{02} = 4 mW/cm^2 (green squares) and I_{03} = 8 mW/cm^2 (blue dots) are presented for gratings recorded at a spatial frequency of 1428 lines/mm. The corresponding prediction of the NPDD model using the best fit parameter values listed in Table 6 are also shown. As can be seen, there is close agreement between the experimental data and the NPDD model predictions.

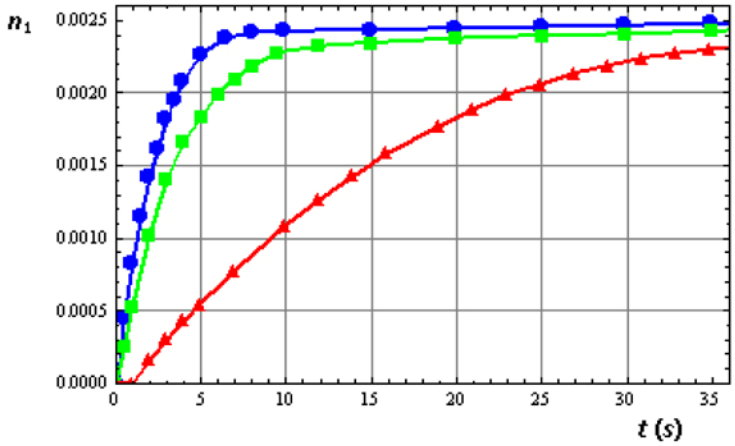

Fig. 3. Growth curves of refractive index modulation recorded in the AA/PVA photopolymer for three recording intensities: I_{01} = 1 mW/cm^2 (red triangles), I_{02} = 4 mW/cm^2 (green squares) and I_{03} = 8 mW/cm^2 (blue circles).

4.2.2 BMS photopolymer

Performing the analogous experiments to those described above in Section 4.2.1 for the AA/PVA case, the BMS photopolymer is examined. Growth curves of refractive index modulation are recorded and monitored for the same three exposing intensities, I_0 = 1 mW/cm^2, 4 mW/cm^2 and 8 mW/cm^2, for the same range of spatial frequencies, 500 – 3000 lines/mm. The transmitted recording beams are monitored, normalised and fit to characterise

#151382 - $15.00 USD Received 26 Jul 2011; revised 5 Sep 2011; accepted 5 Sep 2011; published 9 Dec 2011

the dye used. Table 7 lists some of the absorption related parameter values extracted from fits to these transmission curves recorded for an exposure intensity of I_0 = 8 mW/cm^2 at various spatial frequencies.

Table 7. Parameters extracted from normalised transmission curves over a range of spatial frequencies in the BMS acrylate photopolymer. I_0 = 8mW/cm^2.

Spatial Frequency (lines/mm)	T_0	T_{sf}	ε (×10^8) (cm^2/mol)	ϕ (mol/Einstein)	k_a (cm^3/mols)
500	0.71	0.92	1.165	0.75	0.654
1000	0.70	0.91	1.180	0.80	0.707
1428	0.70	0.90	1.130	0.80	0.645
2000	0.69	0.90	1.150	0.80	0.689
2500	0.69	0.90	1.109	0.83	0.689
3000	0.71	0.91	1.116	0.80	0.637
Mean	**0.70±0.01**	**0.91±0.01**	**1.141±0.039**	**0.80±0.05**	**0.670±0.037**

It can be seen from the table that the estimated parameter values do not vary appreciably as the spatial frequency varies. The average material layer thickness extracted was found to be, d = 26.5 ± 1.5 μm, which is approximately one quarter the thickness of the AA/PVA samples (μm), but the molar absorptivity, ε (cm^2/mol) is very similar. Interestingly the average value obtained for the rate of production of the excited state photosensitiser, k_a (s^{-1}), is almost six times faster than the rate observed in the equivalent AA/PVA case for the same exposure intensity, (8 mW/cm^2). This appears to be as a result of this material's high quantum efficiency, ϕ = 0.8 (mol/Einstein).

The parameter values extracted from fits to the growth curves recorded at the same spatial frequencies are listed in Table 8. For consistency, and to make meaningful comparisons between the two photopolymer materials, the values provided in Table 8 are for fits to growth curves recorded with I_0 = 8 mW/cm^2, as is the case in Table 6 for the AA/PVA material.

Table 8. Parameters extracted from growth curves of refractive index modulation over a range of spatial frequencies in the BMS acrylate photopolymer material.

SF (lines/mm) [n_1^{sat}×10^{-3}]	k_d cm^3/mols (×10^5)	k_p cm^3/mols (×10^7)	k_t cm^3/mols (×10^8)	D_{m0} cm^2/s (×10^{-10})	$\sqrt{\sigma}$ (nm)	MSE (×10^{-10})
500 [2.90]	1.0	2.0	4.5	2.20	9.0	2.22
1000 [5.00]	1.0	1.9	4.2	2.00	9.0	1.23
1428 [7.10]	0.9	2.1	5.0	1.90	10.0	2.10
2000 [7.20]	1.2	2.2	4.4	2.10	11.0	3.40
2500 [8.50]	0.8	1.6	4.8	2.21	8.0	1.80
3000 [8.86]	1.1	2.1	4.4	1.87	8.0	3.11
Mean	**1.0±0.2**	**1.98±0.38**	**4.55±0.45**	**2.5±1.5**	**9.2±1.8**	**2.31±1.09**

Examining the results obtained for each photopolymer, there is little variation between parameter estimates extracted for different spatial frequencies. However, significant differences do exist between the extracted parameters for the different materials; see Table 6 and Table 8. First, we note that the mean value for the rate of dissociation of the initiator, $k_{d\ acrylate}$ = 1.0 × 10^5 (cm^3/mol s) which is two orders of magnitude larger than the equivalent value in the AA/PVA case, i.e., $k_{d\ AA}$ = 1.58 × 10^3 (cm^3/mol s). Considering this and the estimates obtained for the rate of production of the excited state photosensitiser, k_a, in the BMS material, it is clear that the initiation processes present in the BMS photopolymer are

#151382 - $15.00 USD Received 26 Jul 2011; revised 5 Sep 2011; accepted 5 Sep 2011; published 9 Dec 2011

significantly faster than those in the AA/PVA material and will therefore generate primary radicals at a much higher rate, (see flow chart in Fig. 1).

Second, we note that the BMS propagation and termination rates are of the same order of magnitude as those estimated for the AA/PVA material. These results are consistent with the kinetic rate constants reported in the literature for acrylates and acrylamide type monomers [34].

Third, the values obtained for the monomer diffusion coefficient D_{m0} (cm^2/s) in the BMS material are an order of magnitude faster than the equivalent values obtained for the AA/PVA material. This relatively fast diffusion rate implies that monomer will diffuse more rapidly into the bright (monomer depleted) regions of the interference pattern during exposure, replacing monomer already polymerised and resulting in an increase in the concentration of polymer formed and hence an increase in the first harmonic of refractive index modulation generated. This increase in modulation achievable is also aided by the fact that the refractive index of the acrylate monomer, n_m, is much larger than the background refractive index of the material, n_b, (see Table 3). Therefore, in contrast to what happens in the AA/PVA case, in the BMS case the migration of the monomer out of the dark regions of the interference pattern produces a reduction in the average refractive index in the dark regions. This is accompanied by a corresponding increase in the average refractive index of the bright regions, resulting in two simultaneous effects contributing to an increase in the refractive index modulation.

We examine the growth curves and theoretical fits presented in Fig. 4. These have been recorded with exposure intensities I_0 = 1 mW/cm^2 (red triangles), 4 mW/cm^2 (green squares), and 8 mW/cm^2 (blue dots) at 1428 lines/mm in the BMS photopolymer. We note that the dosage required to reach refractive index modulation saturation is considerably less than for the equivalent AA/PVA growth curves which are presented in Fig. 3. This is consistent with the extracted parameter values, which indicate that the acrylate photopolymer's photo-initiation behaviour and diffusion rates are much faster than those of the AA/PVA material.

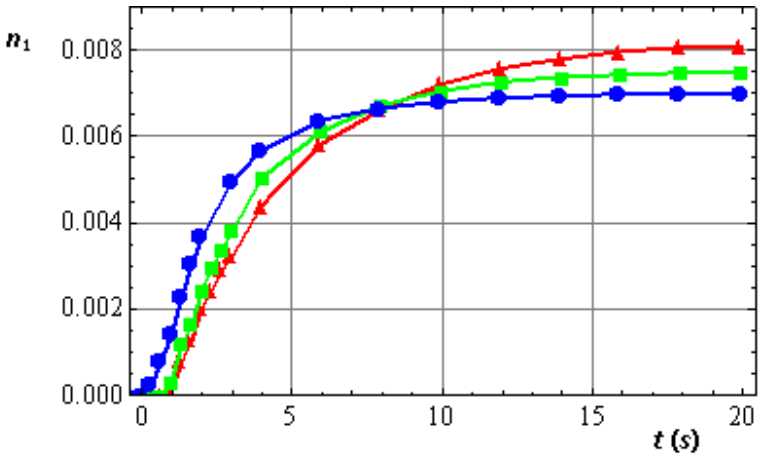

Fig. 4. Growth curves of refractive index modulation recorded in the BMS photopolymer for three recording intensities: I_{01} = 1 mW/cm^2 (red triangles), I_{02} = 4 mW/cm^2 (green squares) and I_{03} = 8 mW/cm^2 (blue circles).

It can be seen from Fig. 4 and Table 6 (first column) that the corresponding refractive index modulation achieved for each intensity and spatial frequency using the BMS material, is much larger than that obtained for the AA/PVA photopolymer. The two major factors contributing to this are the relative refractive indices of the components that constitute the materials (see Tables 3 and 4) and significantly the values obtained for the non-local response parameter.

#151382 - $15.00 USD Received 26 Jul 2011; revised 5 Sep 2011; accepted 5 Sep 2011; published 9 Dec 2011

In Table 6 we see that the estimated mean value obtained for the nonlocal response parameter is $\sqrt{\sigma}$ = 9.2 nm. This value is over six times smaller than the mean value extracted for the AA/PVA photopolymer. This has important consequences, and we recall the prediction of the NPDD model, that a reduction in the extent of the non-local effects in a photopolymer will result in an increase in a material's spatial frequency response. Figure 5 shows the spatial frequency response of both photopolymers using the saturated refractive index modulation values presented in Tables 6 and 8. It can be clearly seen from Fig. 5 that the performance of the BMS photopolymer (blue dots), i.e., spatial frequency response, is superior to that of the standard AA/PVA photopolymer (red squares). It must be noted at this point that reflection geometries are being examined in both media and the observed trend shown here in Fig. 5 holds true [41–43].

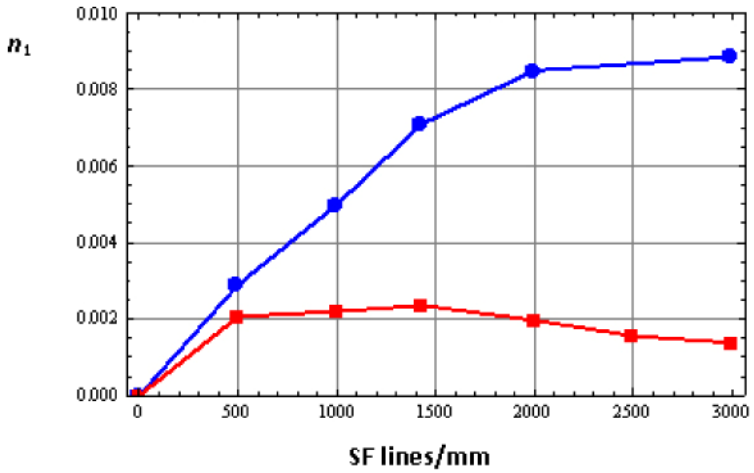

Fig. 5. Comparison of the spatial frequency response of the AA/PVA photopolymer (red squares) and the BMS photopolymer (blue dots). All recordings were carried out with an exposing intensity of I_0 = 8 mW/cm^2.

5. Conclusions

A photopolymer material developed by Bayer MaterialScience was examined using various optical techniques. The material was then characterised using the Non-local Photo-polymerization Driven Diffusion (NPDD) model and its performance contrasted to that of a well known acrylamide/polyvinylalcohol based photopolymer. Based on the observed experimental results, the modelling of the data using the NPDD model's coupled differential equations and the comparison between both photopolymer materials it can be seen that the BMS material has:

(i) A substantially faster response of the refractive index modulation with respect to the recording dosage, especially at lower power densities;

(ii) A three times higher refractive index modulation that is achievable in the composition that was under investigation here compared to the AA/PVA photopolymer;

(iii) A six times smaller the non-local response parameter, $\sqrt{\sigma}$ within the NPDD model representing the spatial spread of the reactive chain ends of the formed polymer coils during photopolymerization, thus indicating the much higher resolution of this Bayer MaterialScience photopolymer;

(iv) An improved performance of the BMS photopolymer material at high spatial frequencies (e.g. reflection holograms) is obtained.

#151382 - $15.00 USD Received 26 Jul 2011; revised 5 Sep 2011; accepted 5 Sep 2011; published 9 Dec 2011

As a result the analysis using the NPDD model qualifies this new material as a very good storage medium for volume holographic recordings.

Acknowledgments

We acknowledge the support of the Irish Research Council for Science, Engineering and Technology through the EMPOWER postdoctoral research programme. We also acknowledge the support of Enterprise Ireland, Science Foundation Ireland through the Research Innovation and Proof of Concept Funds, and the Basic Research and Research Frontiers Programmes. We thank also Ursula Tracht (Bayer TechnologyServices) for fruitful discussions.

#151382 - $15.00 USD Received 26 Jul 2011; revised 5 Sep 2011; accepted 5 Sep 2011; published 9 Dec 2011